High-resolution photoemission mapping of the three-dimensional band structure of Bi(111)

Christian R. Ast* and Hartmut Höchst[†]

Synchrotron Radiation Center, University of Wisconsin-Madison, Stoughton, Wisconsin 53589, USA
(Received 16 December 2003; revised manuscript received 2 July 2004; published 27 December 2004)

Angle-resolved photoemission spectra of Bi(111) excited with synchrotron radiation at photon energies from 9 to 100 eV have been used to determine the initial- and final-state band structures along ΓT. Deviations from the free-electron dispersion for energies below about 60 eV can be accounted for by an energy-dependent extension function to the final-state bands. The experimentally determined dispersion of the top three bulk valence bands is compared with literature data and various band-structure calculations, none of which satisfactorily describes the observed band width, the critical-point energies, or their specific dispersion relations $E_i(k)$. At a photon energy of 29 eV, direct transitions lead to a pronounced final-state gap. In this region, the experimental band-structure map consists of features resembling the one-dimensional density-of-states projection of the Bi bulk band structure onto the (111) surface.

I. INTRODUCTION

Determining the electronic ground- and excited-state properties is a major challenge in theoretical and experimental condensed-matter physics.[1,2] Angular-resolved photoemission spectroscopy (ARPES) is widely regarded as the tool of choice to investigate the electronic structure $E(\vec{k})$ of the occupied valence bands.[3] However, due to the fact that the momentum-resolved-photoemission process is taking place between the initial-state $E_i(\vec{k})$ and the final-state $E_f(\vec{k})$ of the empty conduction band, ARPES measures the combined dispersion effects of both states.

The experimental band structure $E(\vec{k})$ measured in ARPES incorporates effects of the self-energy $\Sigma(\omega)$. Recent attempts in treating the photoemission process in a one-step model produced very good results for some prototypical metal and semiconductors.[4–8] For Bi, however, *ab initio* $\Sigma(\omega)$ calculations are not yet available and experimental photoemission data are thus compared to the more common and simpler model calculations of free-electron-like final-state bands.

We report angle-resolved photoemission spectra of Bi(111) along the ΓT line. In the following, we will demonstrate that the appearance of periodic structures in ARPES measured over a wide photon energy range can be successfully used to extract significant final-state information allowing the dispersion $E_i(\vec{k})$ of bulk valence bands to be determined with high precision.

Using a phenomenological model that incorporates deviations from the free-electron dispersion at lower final-state energies enables us to determine the initial-state bands within 3 eV binding energy as well as the final-state bands up to an energy of 100 eV. Normal emission spectra obtained at lower photon energies display a complex behavior that we assign to secondary cone emission.[9] Previous experimenters noticed the spectral complexity and chose to dismiss valuable information from the spectral range below about 40 eV photon energy.[10] Due to the reduced perpendicular momentum broadening $\Delta k_{f\perp}$ in the final states, ARPES experiments at

lower photon energies are intrinsically more precise in reflecting the true three-dimensional band dispersion and band width than those carried out at higher photon energies.[11] The merits of keeping $\Delta k_{f\perp}$ small will be discussed by comparing our experimental initial-state Bi-band structure data with those published by Jezequel *et al.*[10] which they obtained with photon energies ranging from $\hbar\omega = 37.5$ to 100 eV.

Finally, we present an intensity map of the valence band that was measured along the $\overline{\Gamma M}$ line at a photon energy of 29 eV. We will show that at this photon energy there is an energy gap in the final state, so that the photoemission intensity can be interpreted as a one-dimensional (1D) density of valence band states (DOS) parallel to the normal emission direction ΓT.

II. ELECTRONIC STRUCTURE

The structure and electronic properties of the semimetal bismuth have been discussed in detail elsewhere.[12–14] In brief, bismuth crystallizes in the rhombohedral arsenic ($A7$) structure with two atoms in the basis. The valence electron configuration of the group-V element is $6s^2 6p^3$. With five valence electrons per atom and two atoms per primitive cell, bismuth should be an insulator. However, the small distortion of the crystal lattice along the [111] direction results in an overlap of the conduction band with the valence band and causes the high symmetry points (T points) at the zone boundary along the [111] direction (trigonal axis) to be inequivalent to the L points. As a result, Bi is a semimetal with minuscule cigar shaped bulk Fermi surface pockets located at the T points (holes) and the L points (electrons).

The geometry of the Bi crystal lattice leads to the formation of bilayers along the (111) plane with weak bonding between them.[15] Therefore, single crystals of bismuth preferentially cleave in the (111) plane. However, Bi is not a layered crystal as it has a fully developed three-dimensional band structure. ARPES measurements of Bi along the [111] direction sample the Brillouin zone of the bulk along the ΓT line. The surface Brillouin zone for Bi(111) is hexagonal and
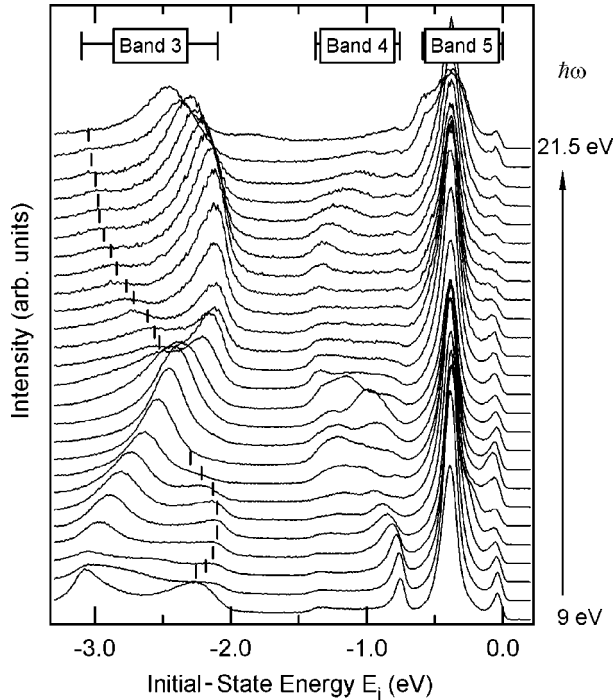
FIG. 1. Energy distribution curves of Bi(111) at normal emission as a function of photon energy from 9 to 22 eV in 0.5 eV steps. The prominent nondispersing peak at -0.4 eV is due to a two-dimensional state. The dispersing peaks can be attributed to bulk states.

off normal emission towards high-symmetry points samples $\vec{k}_{\parallel}$ along the $\overline{\Gamma M}$ and $\overline{\Gamma K}$ lines.

III. EXPERIMENTAL DETAILS

The photoemission experiment was performed at the Synchrotron Radiation Center of the University of Wisconsin-Madison in Stoughton, Wisconsin. Measurements were done using the 4-m normal incidence monochromator (4mNIM) beamline as well as the undulator plane grating monochromator (U-PGM) beamline. Single crystals of bismuth were cleaved *in situ* revealing a clean (111) surface and kept at a pressure $<8 \times 10^{-11}$ Torr. The total energy resolution of the photoemission spectra was usually set to 40 meV. The angular resolution was $\pm 0.5°$. In order to minimize phonon related broadening in the spectra (Debye temperature of Bi: 120 K) the sample temperature was set to 50 K. Additional experimental details are given elsewhere.[16]

IV. RESULTS AND DISCUSSION

A. Normal emission spectra

In Fig. 1 energy-distribution curves (EDC's) of Bi(111) at normal emission are shown for photon energies ranging between 9 and 22 eV in 0.5 eV steps. The most prominent feature in the spectra is a nondispersing peak at about -0.4 eV, which can be attributed to a two-dimensional state.[15] Within the measured binding energies the photoemission spectrum exhibits three p-like bulk bands.[13,14,17,18] The range
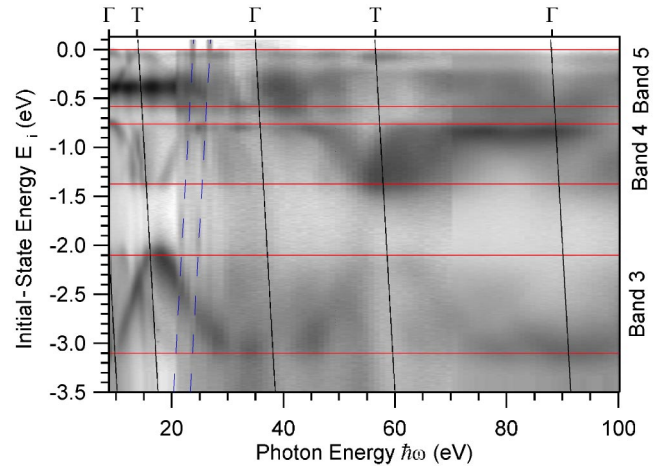

FIG. 2. (Color online) Intensity map of energy distribution curves of Bi(111) at normal emission. The band width of the top three valence bands are outlined by red lines. The blue dashed lines indicate $5d$ core level emission from second order light. The points of high symmetry are indicated by black quasivertical lines.

of dispersion of these bands labeled bands 3, 4, and 5 is indicated. Photoemission from the two lower lying s-like bands (bands 1 and 2) with $E_i \approx -14$ eV and ≈ -10 eV is much weaker at these low excitation energies and is not shown in Fig. 1. Particularly noteworthy is the behavior in the energy region between -3 and -2 eV. In this energy range we observe multiple emission features with opposite dispersion directions. The dispersion of the weaker emission feature is indicated by vertical markers. Since there is only one initial-state band in this region, the conclusion is that they are due to transitions into other final-state bands, i.e., secondary-cone emission. Previous angle-resolved photoemission studies on Bi(111)[10,15,19-23] were primarily concerned with the off-normal dispersion of surface states or resonances. The only other experiments reporting photon-energy-dependent ARPES data along the ΓT direction are from Jezequel *et al.*[10] Their spectra are noticeably less structured with a much higher inelastic background. The emission from the two-dimensional band is hidden in a 1.5 eV wide multicomponent peak which is of the same magnitude as that from band 3 at an initial-state energy of about 3 eV, while our spectra show a relative increase of emission intensity from the two-dimensional band by more than three times as well as a clear separation of transition features assigned to bands 4 and 5 of the bulk band structure. The significantly improved spectral quality of our data is most likely the result of a combination of higher energy and slightly better momentum resolution, a reduced intrinsic broadening due to the surface quality of the crystal, as well as a reduced electron-phonon interaction at temperatures well below the Debye temperature.

The experimental band structure is visualized in Fig. 2 where we display the ARPES intensity as a function of photon energy ranging from 9 to 100 eV. To enhance weaker features in the spectrum the intensity scale is logarithmic. Light and dark areas correspond to low and high intensities, respectively. The variations in photoemission intensities reflect matrix element dependencies on the photon energy, the

polarization of the photons, and the character of the initial and final states.[24]

Emission from bands 3, 4, and 5 in Fig. 2 is separated by distinct horizontal stripes of low-photoemission intensity as indicated by the horizontal red lines. These low intensity stripes can be related to energy gaps in the initial-state band structure. A general periodic behavior can be observed for all bands indicating that multiple Brillouin zones are covered. The tilted black lines show the location of the high-symmetry points Γ and T. Furthermore, the bands do not appear as continuous emission features but are interrupted by stripes of low-photoemission intensity which are parallel to the high-symmetry lines. These quasivertical stripes are direct evidence of energy gaps in the final-state band structure.

The intensity of the two-dimensional state at E_i $=-0.4$ eV is noticeably stronger in the lower photon energy range.[15] The dashed lines in Fig. 2 mark the trace of the $5d$-core levels in Bi. They appear in the spectra due to presence of second order radiation from the monochromator. The origin of these features can be easily verified as they are also present above the Fermi level, i.e., for initial-state energies ($E_i > 0$).

B. Final-state symmetry points and band structure

The final-state bands can be iteratively determined from the normal-emission spectra in Fig. 2. The starting point for identifying a nonfree electron final-state (non-FEFS) band is to locate the maxima and minima (i.e., the high symmetry points) in the initial-state band structure as a function of photon energy. These values are used for the first approximation of the final-state bands from which the full initial-state dispersion in momentum space can be extracted. The process repeats by using the initial-state bands to obtain more refined final-state bands until a best fit to the data points is obtained. Figure 3 shows the experimental final-state bands obtained by the iterative method. The circles labeled $G1$–$G4$ indicate gaps in the emission due to avoided crossings between the primary cone emission band $F1$ (solid line) and the two bands $F2$ and $F3$ (dashed lines) associated with secondary cone emission. Towards higher final-state energy the bands follow the free electron dispersion with a potential offset of $E_0=-9.7$ eV and an effective mass of $0.91m_e$. A list of final-state energies and experimentally obtained band gaps for the symmetry points Γ and T in Bi(111) are shown in Table I.

At lower final-state energies the final-state bands do not follow a simple FEFS dispersion. To account for the energy-dependent deviations in $E_f(\vec{k}_f)$ we used the following empirical extension of the FEFS model:

$$E_f(\vec{k}_f) = \frac{\hbar^2}{2m^*}(\vec{k}_f + \vec{G})^2 \cdot f(\vec{k}_f, \vec{G}) + E_0, \qquad (4.1)$$

where m^* is the effective mass, E_0 is the potential offset defined as the energy difference between the band minimum and the Fermi level, and $\vec{k}_f$ is the final-state momentum in the reduced zone scheme. Equation (4.1) is very similar to the free-electron model except that a function $f(\vec{k}_f, \vec{G})$ has been included to account for energy-dependent deviations from
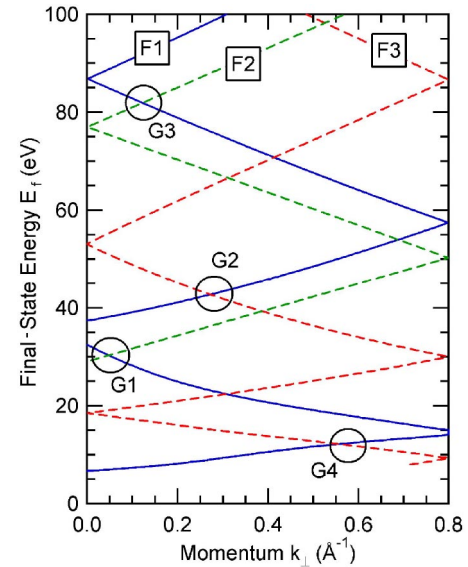

FIG. 3. (Color online) Experimental final states for Bi along the Γ𝑇 line as extracted from the data. Solid and dashed lines indicate bands participating in primary-(blue) and secondary-cone emission (red and green), respectively. The circles labeled $G1$–$G4$ indicate gaps due to avoided final-state crossings.

the free-electron model. As the energy increases this function has to approach unity to be consistent with the FEFS model at higher final-state energies. In this model energy gaps have been generally neglected as they require more detailed measurements in the vicinity of the gaps.

The FEFS extension function $f(\vec{k}_f, \vec{G})$ is the result of the iterative process to provide a best fit to the data in Fig. 5. It intersects all of the critical point energies given in Table I. The energy dependence of $f(\vec{k}_f, \vec{G})$ of the FEFS is shown in Fig. 4(a) in blue for the primary-cone emission band and in red for the secondary-cone emission band. The other secondary-cone emission band (green band in Fig. 5 turns out to be free-electron-like within the error limits. For higher energies above 60 eV the FEFS extension function approaches unity (vertical dashed line). The dispersion of the experimentally determined final-state bands is plotted in Fig. 4(b) in the extended zone scheme. For comparison we show

TABLE I. Experimentally determined critical point energies E_f in eV for the final-state bands along Γ𝑇. The curly brackets indicate energy gaps at particular symmetry points.

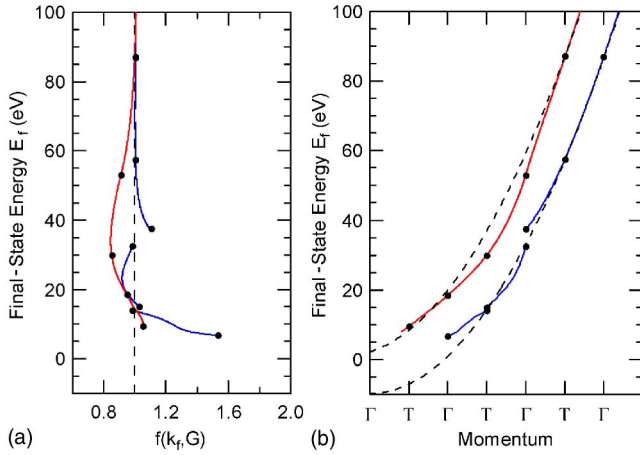| Symmetry point	$F1$	$F2$	$F3$
Γ	6.7		
𝑇	$\begin{cases} 14.0 \\ 15.0 \end{cases}$		9.25
Γ	$\begin{cases} 32.5 \\ 37.5 \end{cases}$	29.1	18.5
𝑇	57.4	50.2	30.0
Γ	87	77	53
𝑇			86.7

FIG. 4. (Color online) The energy-dependent extension of the FEFS $f(\vec{k}_f, \vec{G})$ is shown in (a) for the primary-cone emission band in blue and for a secondary-cone emission band in red. A comparison of the final-state band dispersion in the extended zone scheme with the respective FEFS bands is shown in (b). The black dots indicate the locations of critical points as listed in Table I.

the dispersion of the FEFS bands as dashed lines. The assignment and color scheme of the solid lines is the same as in Fig. 4(a). The black dots are the experimentally determined critical points of the final-state bands (see Table I).

The analysis shows that in the energy range, where deviations from the FEFS model occur, an energy-dependent modulation of the FEFS provides an adequate description of the final-state energy bands. Even though emission intensities for different features in the spectra vary as a function of photon energy, the position of emission features can be clearly assigned to primary- and secondary-cone emission.

Figure 5 shows the intensity image of band 3 as a function of photon energy. The black dots denote the peak positions of the ARPES scans in the energy region $E_i = -3.2$ to -2 eV.
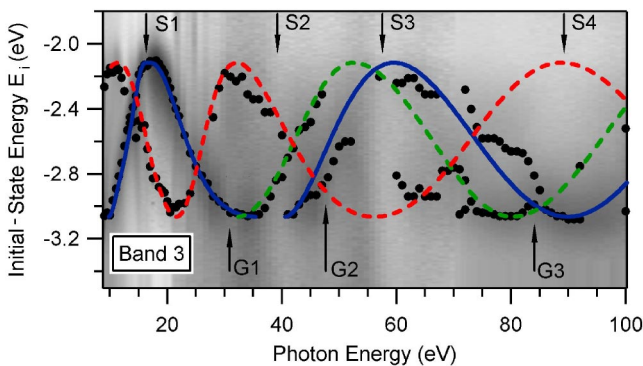

FIG. 5. (Color online) Intensity image of the normal emission spectra of band 3 as a function of photon energy. The black dots show the peak positions from the individual ARPES energy scans. The colored lines show the dispersion of the initial-state bands as a function of photon energy. The solid line (blue) corresponds to primary-cone emission while the dashed lines (red and green) correspond to secondary-cone emission. The emission gaps $G1$ to $G3$ are related to avoided final-state crossings as indicated in Fig. 3(b). The emission gaps $S1$–$S4$ correspond to the band gaps at the symmetry points Γ and T (see Fig. 2).

For spectra measured with photon energies ranging from 9 to 22 eV the peak positions have been determined by fitting the data to a model spectrum consisting of Lorentzians, a background function[25] and a Fermi-Dirac distribution function. For photon energies larger than 22 eV the peak positions have been determined solely by the peak maxima. The lines which are drawn through the data points follow the same color coding as those in Fig. 3. For photon energies below 40 eV secondary-cone emission (red line) accompanies the primary-cone emission (blue line) with a dispersion relation that is nearly opposite in phase to that of the primary-cone transitions. Due to emission gaps at higher energies and the increase in lifetime width, an assignment to primary- or secondary-cone transitions is getting less obvious particularly towards the upper end of the spectral range.

C. The initial-state band structure

Commonly, the desired information from ARPES is the valence band dispersion $E(\vec{k})$. However, the experimental band structure $E(\vec{k})$ is subject to many body effects incorporated in the self-energy $\Sigma(\omega)$: $E(\vec{k}) = \epsilon(\vec{k}) + \text{Re}\Sigma(\omega)$, where $\epsilon(\vec{k})$ is the one electron band structure of the noninteracting system. *A priori*, it is not clear to which extend and over which energy range correlation effects will affect the one electron band structure of a system such as the semimetal Bi. In general, many body effects can lead to a reduced band width of the initial states and cause dispersion deviations near the Fermi level.[16,26,27] A recent model calculation based on the GW formalism showed that photoemission data of Cu, which can be considered as a prototype weakly correlated system, can be quantitatively described within the single quasiparticle approximation.[8] With the final-state bands which we established in the previous section we have the proper $k_\perp$ values for the ARPES peaks which yields the valence band dispersions $E_i(\vec{k})$.

The transition energies of the top three valence bands covered in Fig. 1 can be extracted along the ΓT direction from peak positions fitted to the normal emission spectra. Figure 6 shows a representative valence band spectrum measured at a photon energy $\hbar\omega = 11.5$ eV and the result of a free fit to multiple Lorentzians including a Shirley-type background[25] and a Fermi-Dirac cut off function. Considering the simplicity of simulating the entire spectrum consisting of seven clearly identifiable peaks within 3 eV initial-state energy, it is surprising how well not only the peak positions but also in most cases their line shapes and widths are simulated. The analysis revealed two nondispersive bands in the region up to -0.5 eV that can be assigned to two-dimensional states originating from the surface or from Bi bilayers.[15] All other peaks can be assigned to three-dimensional bulk bands as a result of either primary-cone emission (PCE) or secondary-cone emission (SCE).

Figure 6 shows also a valence band spectrum measured at $\hbar\omega = 14$ eV. At this photon energy for band 4 the secondary-cone emission is stronger than the primary-cone emission. This enhancement is the result of final-state hybridization due to the avoided crossing $G4$ as indicated in Fig. 3. The
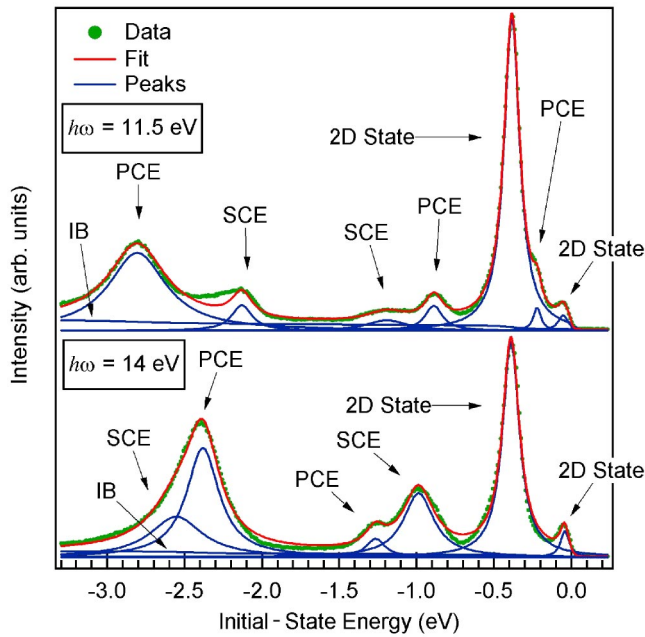
FIG. 6. (Color online) Energy-distribution curve at a photon energy of 11.5 and 14 eV along with Lorentzian line shapes fitted to primary- (PCE) and secondary-(SCE) cone emission features as well as an inelastic background (IB).

relative increase in emission intensity in the photon energy region close to $\hbar\omega=14$ eV can be seen in the band-structure image in Fig. 7(a) where normal-emission spectra are shown for low photon energies between 9 and 22 eV. The experimental peak dispersions (filled dots: PCE, open dots: SCE)

follow the respective dispersion branches of the primary- (dashed blue line) and secondary-emission features (dashed red line) which were calculated by assuming a band gap of 1 eV at $G4$. The dispersion is almost vertical near $\hbar\omega=14$ eV indicating the strong hybridization which enhances the SCE peak.

Figure 7(b) shows the dispersion of the top three valence bands along ΓT. The data points come from spectra at photon energies between 9 and 22 eV. The two data points in bands 4 and 5 at the Γ point were taken at a photon energy of 32 eV. The solid lines are best fits to the individual bands using a superposition of cosine functions. For clarity we selected to display only the data points associated with the direct transitions. The data points related to transitions into the secondary-cone emission bands follows the same general dispersion relation.

Figure 7(c) compares our band dispersion with the data published by Jezequel *et al.*[10] Due to the complexity of their spectra below $\hbar\omega=40$ eV, they chose to process only spectra at higher energies. Their valence band dispersion differs from our data. Most noticeably emission from the topmost band (band 5) is completely missing and emission points which we assigned to band 3 were nondispersive over about one third of the Brillouin zone (triangles) and incorrectly associated to processes related to the sample surface. We think that the discrepancies, an initially nondispersive band which starts out above the true band minimum followed by a steep dispersive part that ends prior to the true band maximum is directly related the experimental conditions under which these data were obtained. The intrinsic final-state momentum broadening $\Delta k_{f\perp}$ increases significantly in the region of the escape depth minimum. The ramifications of an
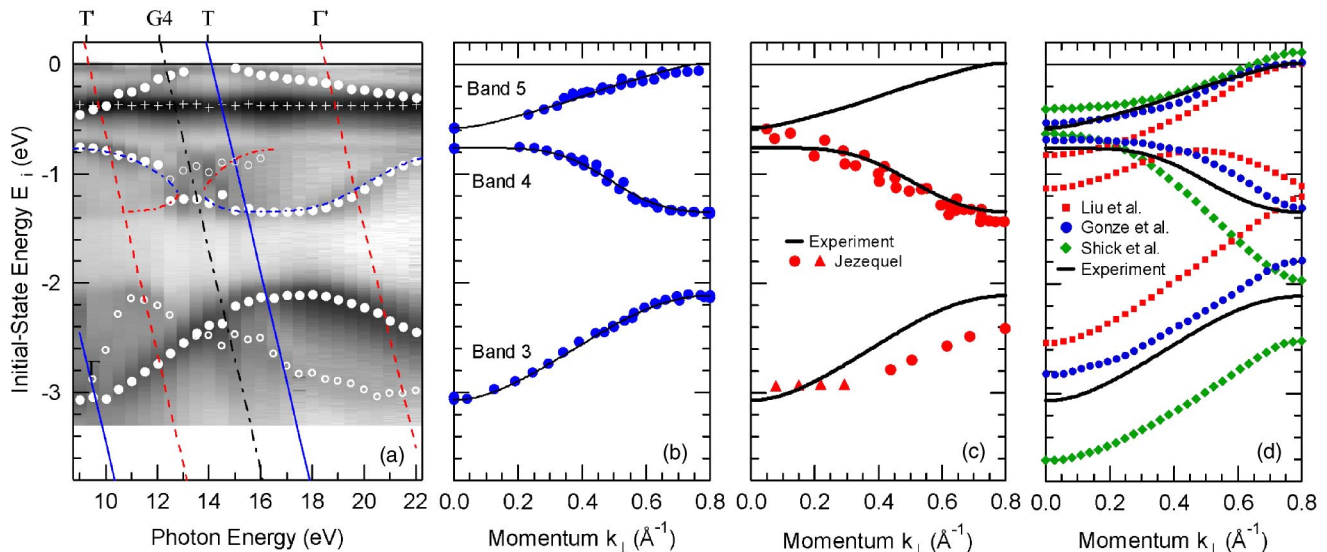

FIG. 7. (Color online) Dispersion of the bulk initial-state bands: (a) Intensity map of valence band spectra between 9 and 22 eV showing the experimental peak dispersion of primary- and secondary-cone emission features as filled and open circles. Final-state hybridization due to the gap opening $G4$ enhances the secondary-cone emission near $\hbar\omega=14$ eV. The crosses indicate the dispersionless 2D state. (b) Valence band dispersion along the ΓT line. The solid line shows a fit through the data points using a superposition of cosine functions. The two data points at Γ for bands 4 and 5 have been extracted at a photon energy of 32 eV. (c) Comparison of the dispersion of the top three valence bands (solid lines) with literature data by Jezequel *et al.* (Ref. 10). (d) Comparison of the experimentally determined valence band dispersion (black lines) with selected theoretical calculations by Schick *et al.* (Ref. 18) (green diamonds), Liu *et al.* (Ref. 14) (red squares) and Gonze *et al.* (Ref. 17) (blue dots).

TABLE II. Initial-state energies E_i in eV at selected critical points in comparison with other experiments and theoretical calculations. For our measurements we estimate an error smaller than ± 0.01 eV.

Γ_6^+	Γ_6^+	Γ_{45}^+	T_6^-	T_6^+	L_a	L_s	Reference
-3.05	-0.76	-0.58	-2.11	-1.35	-2.10	-2.19	this work
-2.90	-0.60	-0.25	-2.30	-1.50			10
-2.83	-0.71	-0.54	-1.80	-1.30	-1.87	-1.96	17
-2.54	-1.13	-0.82	-1.18	-1.12	-1.67	-1.79	14
-3.61	-0.62	-0.39	-2.50	-1.98	-2.41	-2.56	18

increased intrinsic $\Delta k_{f\perp}$ in ARPES at higher photon energies which should not be confused with the instrumental $\Delta k_\parallel$ resolution, are nicely summarized in a recent review article by Strocov.[11] At lower photon energies the sampling width over the Brillouin zone is relatively small, a prerequisite for meaningful ARPES enabling the point-by-point sampling of the dispersive branch of three-dimensional bands, particularly near band extrema or at Fermi level crossings. For the data shown in Fig. 7(b) we estimate the final-state momentum broadening to be less than 15% of the Brillouin zone along ΓT, which is reasonably small for three-dimensional band mapping.

A comparison of the experimental valence band dispersion (black lines) with three different theoretical calculations is shown in Fig. 7(d). Included are a third neighbor empirical tight binding calculation by Liu *et al.* (red squares),[14] an *ab initio* first principle calculation by Gonze *et al.* (blue dots),[17] as well as a relativistic total energy calculation by Shick *et al.* (green diamond).[18] For all three bands we notice significant deviations from the experimental critical point energies at Γ and T as well as in the general dispersion relation. This observation is somewhat surprising since at least the semiempirical calculation by Liu *et al.* used experimental data for the parametrization of the Hamiltonian matrix elements. Interestingly, the model calculation which comes closest in describing the measured band dispersion is the *ab initio* first principle calculation by Gonze *et al.*[17] while the most recent relativistic band structure based on the local density approximation (LDA) misrepresents the photoemission band onsets of band 3 as well as the onsets and dispersion of band 4 along the [111] direction of Bi.[18] The experimental critical point energies are listed in Table II and compared with other experimental and theoretical predictions. It is not obvious if the apparent discrepancies are the result of shortcomings in the theoretical one-electron band structure models or rather reflects the fact that self-energy effects cannot be ignored in the ARPES analysis of Bi.

D. Projected bulk band structure

An interesting situation occurs in ARPES when the excited state falls into a band-gap region. From the simplistic discussion of the photoemission process presented earlier in this paper one would think that the photoemission intensity simply vanishes. This is the case for the momentum-resolved direct transitions. However, evanescent final states which penetrate particularly deep into the bulk in gapped regions

also participate in the photoemission process and ARPES then samples over the entire valence band, essentially outlining the region of occupied states along a particular momentum direction perpendicular to the (111) surface.

A photoemission intensity map measured with 29 eV photons resulting in final-state gap transitions from gap $G1$ (see Fig. 3 is shown in Fig. 8. The parallel component of the momentum is along the $\overline{\Gamma M \Gamma}$ line of the Bi(111) surface Brillouin zone. The intensity scale is linear, where light and dark colors correspond to low- and high-photoemission intensity, respectively. Up to $E_i \approx -0.75$ eV well-defined emission features can be seen in the vicinity of the $\overline{\Gamma}$ points. These features are associated with the two-dimensional bands of the (111) surface bilayer.[15] The energy region displayed in Fig. 8 covers three bulk valence bands, however, only two are visible in the image. Band 5, which is closest to the Fermi level, cannot be seen in the spectra due to relativistic dipole selection rules.[13,28] For energies $E_i < -0.75$ eV one notices very broad emission features extending along the $\overline{\Gamma M \Gamma}$ line. Emission bands start at the $\overline{\Gamma}$ points dispersing towards higher energy as they approach the $\overline{M}$ point. Near the $\overline{M}$ point they abruptly change into a more intense triangularly shaped pattern.
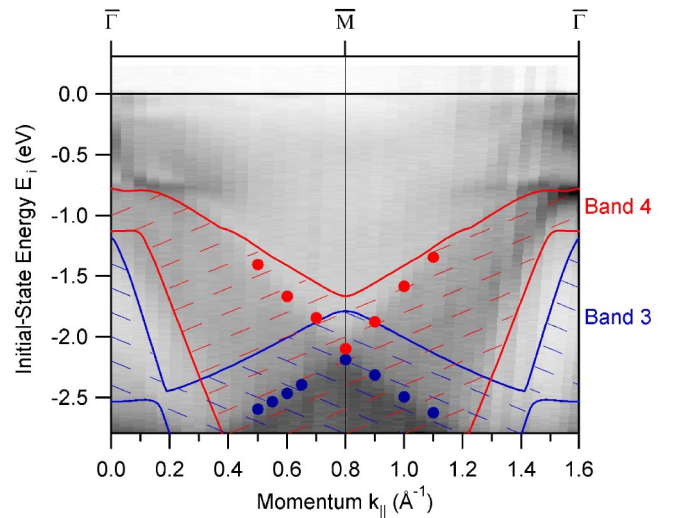

FIG. 8. (Color online) Band structure map along $\overline{\Gamma M \Gamma}$ at a photon energy of 29 eV. Due to a final-state gap at this photon energy the emission features outline the region of occupied states. The leading edges of the broad emission features are indicated by red and blue circles. The hatched areas correspond to the projected band structure from a calculation by Liu *et al.* (Ref. 14).

For comparison we also show the hatched outlines of the projected band structure of bands 3 and 4 of Bi(111). The crosshatched area outlines the region where the two projected bands overlap. The calculation is based on the tight-binding parameters of Liu *et al.*[14] Even though the tight-binding approach did not provide the best fit to the data shown in Fig. 7, the projected band structure conveys the main information needed to discuss the special ARPES features from emission into a final-state gap. Thus, the broad emission features can be associated with the region of occupied states replicating the one-dimensional (ID) density of states (DOS) along the perpendicular momentum direction.

The dispersion of band 4 in Fig. 8 agrees reasonably well with the data close to the $\overline{\Gamma}$ points. Moving away from the $\overline{\Gamma}$ points towards the $\overline{M}$ point, however, the area outlined by the projected band deviates from the experimental data. The discrepancy gradually increases and is largest at the $\overline{M}$ point where the projected band moved about 0.43 eV closer to the Fermi level.

Band 3 in Fig. 8 does not coincide with the broad emission feature at the $\overline{M}$ point. The energy E_i is about 0.4 eV higher than what our data suggest. However, the area and shape covered by both bands near the $\overline{M}$ point coincides with the triangular emission feature. In this region, the two projected bands overlap and both initial-state bands are part of the photoemission process resulting in increased photoemission intensity. Neglecting the energy shifts necessary for the calculated projection to coincide with the experimental data, the geometrical shape of the calculated areas outlines the measured occupied states fairly well.

The upper edge of the projected band structure at the $\overline{M}$ point coincides with the location of the L point. Therefore, the initial-state energy for the leading edges of the two broad emission features indicated by the blue and red circles at the $\overline{M}$ point in Fig. 8 correspond to the initial-state energies of bands 3 and 4 at the L point, i.e., L_s and L_a, respectively. The experimental energy values are displayed in Table II in comparison with theoretical calculations.

V. CONCLUSIONS

The final- and initial-state band structure of Bi(111) along the ΓT direction have been extracted from photon-energy-dependent ARPES data at normal emission. For final-state energies less than 60 eV the bands show significant deviations from the FEFS dispersion. The dispersion can be modeled by using an empirical energy-dependent extension function. This function asymptotically approaches a free-electron parabola with an inner potential of $E_0 = -9.7$ eV and an effective mass of $0.91 m_e$.

Normal-emission spectra show transitions from a particular initial-state into multiple final states. In addition, hybridization between primary- and secondary-cone emission bands prevents band crossings resulting in energy gaps within the Brillouin zone that weakens direct transitions from these regions.

For the initial-state bands we determined the dispersion $E_i(\vec{k})$ of the three valence bands closest to the Fermi level. A comparison with other experimental data and various theoretical model calculations shows noticeable discrepancies in the critical-point energies as well as in the dispersion relation of individual bands. While the discrepancy with the experimental data by Jezequel *et al.* seem to be the related to the increased perpendicular momentum broadening which reduces the intrinsic accuracy of their data analysis, the shortcomings towards various theoretical calculations cannot be as easily identified. At this point we cannot comment on whether the discrepancy with theoretical predictions is a result of many-body effects in the photoemission spectra or related to shortcomings of the different bulk band structure calculations of Bi.

A band structure map measured along the $\overline{\Gamma M}$ line at a photon energy of 29 eV leads into a final-state gap. The resulting spectra show an outline of the region of occupied valence band states. The emission intensity can be interpreted as the 1D-DOS of valence band states along lines parallel to ΓT. Regions in which the projections of two bands overlap can be identified in the spectra as areas of increased photoemission intensity.

---

*Present address: Max-Planck-Institut für Festkörperforschung, Heisenbergstraße 1, D-70569 Stuttgart, Germany

†Email address: hhochst@facstaff.wisc.edu

[1] F. Aryasetiawan and O. Gunnarsson, Rep. Prog. Phys. **61**, 237 (1998).

[2] *Solid-state Photoemission and Related Methods: Theory and Related Methods* edited by W. Schattke and M. A. V. Hove, (Wiley, New York, 2003).

[3] S. Hüfner, *Springer Series in Solid-State Sciences*, 2nd ed. (Springer-Verlag, Berlin, 1996), Vol. 82.

[4] R. Courths, S. Lobus, S. Halilov, T. Scheunemann, H. Gollisch, and R. Feder, Phys. Rev. B **60**, 8055 (1999).

[5] T. Strasser, C. Solterbeck, W. Schattke, I. Bartos, M. Cukr, P. Jiricek, C. S. Fadley, and M. A. VanHove, Phys. Rev. B **63**, 195321 (2001).

[6] L. Plucinski, R. L. Johnson, B. J. Kowalski, K. Kopalko, B. A. Orlowski, Z. D. Kovalyuk, and G. V. Lashkarev, Phys. Rev. B **68**, 125304 (2003).

[7] V. N. Strocov, R. Claessen, F. Aryasetiawan, P. Blaha, and P. O. Nilsson, Phys. Rev. B **66**, 195104 (2002).

[8] A. Marini, G. Onida, and R. DelSole, Phys. Rev. Lett. **88**, 016403 (2001).

[9] G. D. Mahan, Phys. Rev. B **2**, 4334 (1970).

[10] G. Jezequel, J. Thomas, and I. Pollini, Phys. Rev. B **56**, 6620

(1997).

[11] V. N. Strocov, J. Electron Spectrosc. Relat. Phenom. **130**, 65 (2003).

[12] V. S. Edel'man, Adv. Phys. **25**, 555 (1976).

[13] S. Golin, Phys. Rev. **166**, 643 (1968).

[14] Y. Liu and R. E. Allen, Phys. Rev. B **52**, 1566 (1995).

[15] C. R. Ast and H. Höchst, Phys. Rev. B **67**, 113102 (2003).

[16] C. R. Ast and H. Höchst, Phys. Rev. B **66**, 125103 (2002).

[17] X. Gonze, J.-P. Michenaud, and J.-P Vigneron, Phys. Rev. B **41**, 11 827 (1990).

[18] A. B. Shick, J. B. Ketterson, D. L. Novikov, and A. J. Freeman, Phys. Rev. B **60**, 15 484 (1999).

[19] J. Thomas, G. Jezequel, and I. Pollini, J. Phys.: Condens. Matter **11**, 9571 (1999).

[20] A. Tanaka, M. Hatano, K. Takahashi, H. Sasaki, S. Suzuki, and S. Sato, Phys. Rev. B **59**, 1786 (1999).

[21] F. Patthey, W. D. Schneider, and H. Micklitz, Phys. Rev. B **49**, 11 293 (1994).

[22] M. Hengsberger, P. Segovia, M. Garnier, D. Purdie, and Y. Baer, Eur. Phys. J. B **17**, 603 (2000).

[23] C. R. Ast and H. Höchst, Phys. Rev. Lett. **91**, 197602 (2003).

[24] M. Lindroos, S. Sahrakorpi, and A. Bansil, Phys. Rev. B **65**, 054514 (2002).

[25] D. A. Shirley, Phys. Rev. B **5**, 4709 (1972).

[26] T. Valla, A. V. Fedorov, P. D. Johnson, and S. L. Hulbert, Phys. Rev. Lett. **83**, 2085 (1999).

[27] A. Eiguren, B. Hellsing, F. Reinert, G. Nicolay, E. V. Chulkov, V. M. Silkin, S. Hüfner, and P. M. Echenique, Phys. Rev. Lett. **88**, 066805 (2002).

[28] G. Borstel, M. Neumann, and M. Wöhlecke, Phys. Rev. B **23**, 3121 (1981).